Applied Surface Science 258 (2012) 9461–9465

Contents lists available at SciVerse ScienceDirect

Applied Surface Science

journal homepage: www.elsevier.com/locate/apsusc

Modelling nanoparticles formation in the plasma plume induced by nanosecond pulsed lasers

M. Girault[a,b], L. Hallo[c,b,*], L. Lavisse[a], M.C. Marco de Lucas[a], D. Hébert[c], V. Potin[a], J.-M. Jouvard[a]

[a] Laboratoire Interdisciplinaire Carnot de Bourgogne (ICB), UMR 6303 CNRS-Université de Bourgogne, 9 Av. A. Savary, BP 47 870, F-21078 Dijon Cedex, France.
[b] Centre Lasers Intenses et Applications (CELIA), Université de Bordeaux 1, 43 rue Pierre Noailles, Talence, France.
[c] CEA CESTA, 15 Avenue des Sablières CS 60001, 33116 Le Barp Cedex, France

ARTICLE INFO

Article history:
Available online 25 April 2012

Keywords:
Laser processing
Nanopowders
Modeling

ABSTRACT

Nanoparticles formation in a laser-induced plasma plume in the ambient air has been investigated by using numerical simulations and physical models. For high irradiances, or for ultrashort laser pulses, nanoparticles are formed by condensation, as fine powders, in the expanding plasma for very high pairs of temperature and pressure. At lower irradiances, or nanosecond laser pulses, another thermodynamic paths are possible, which cross the liquid–gas transition curve while laser is still heating the target and the induced plasma. In this work, we explore the growth of nanoparticles in the plasma plume induced by nanosecond pulsed lasers as a function of the laser irradiance. Moreover, the influence of the ambient gas has also been investigated.

1. Introduction

Nanopowders formation is frequently observed by interaction of table-top pulsed lasers with a target. The energy deposited by the laser beam at the target surface, gives rise to a shock wave followed by an ablation front in the target [1–3]. In the nanosecond regime, laser ablation produces a thin liquid layer followed by the expansion of a plasma in the ambient gas, i.e. the plasma plume. For high laser irradiances, $I_p \gtrsim 10^{10}\,W\,cm^{-2}$, or ultrashort laser pulses, ablation is often accompanied by nanoparticles (or nanopowders) formation [4]. Usually, the final plasma temperature exceeds a critical value and nanopowders are mainly composed of particles formed by condensation [5,6].

For low laser irradiances, $10^5 \lesssim I_p \lesssim 10^8\,W\,cm^{-2}$, or very long laser pulses, laser energy may be just enough to melt and then to vaporize the matter in the target surface. In this regime, solid matter and heated layer are separated by a sharp boundary. The temperature gradient in this boundary remains quasi-constant during the laser energy absorption, and the solid/liquid interface can expand toward the ambient gas. Observations of the target after laser irradiation usually show surface modifications and small holes due to direct ejection of liquid fragments.

For intermediate intensities, $10^8 \lesssim I_p \lesssim 10^{10}\,W\,cm^{-2}$, combined effects are observed, and the expanded vapor can contain liquid fragments. The expanding mixture can follow a complex thermodynamic path which crosses the saturation curve (i.e. the binodal) up to the gas state, then it expands adiabatically and gives rise to the growth of powders by condensation. Analytical solutions of such flows are difficult to be obtained because the absorption coefficient depends on the target state. Indeed, reflectivity decreases with temperature, thus absorption becomes higher at the end of the laser pulse. Modeling of such processes requires realistic equations of state (EOS) as well as an accurate knowledge of the thermal and thermodynamic properties of the target. For these reasons, numerical simulations are required.

In this work, the 1D hydrodynamic code ESTHER [7] was used to study the properties of the plasma induced by a nanosecond laser shot on a metal target in order to obtain realistic thermodynamic paths followed by the plasma plume during and after the laser pulse. By this method, we analyze the influence of the laser treatment conditions, namely the laser irradiance and the ambient gas nature, and we address the possibility to obtain nanoparticles by condensation. Finally, experimental observations of the nanopowders collected during the laser irradiation of a titanium target are reported and compared to numerical simulations.

2. Experimental and simulation details

Nanopowders were obtained by surface laser treatment in the ambient air of a commercially pure titanium target with a Kaluti System Nd:YAG laser ($\lambda = 1064$ nm, full-width at half-maximum (FWHM) of the laser pulse $\tau_p = 40$ ns). Powders were collected on glass plates placed close to the target. The collected powders were studied by scanning electron microscopy (SEM) and transmission

* Corresponding author. Tel.: +33 557044509.
E-mail address: hallo@celia.u-bordeaux1.fr (L. Hallo).

0169-4332/$ – see front matter © 2012 Elsevier B.V. All rights reserved.
http://dx.doi.org/10.1016/j.apsusc.2012.04.117

electronic microscopy (TEM)[8]. Raman spectroscopy and TEM in diffraction mode were used for the structural characterizations.

The laser energy deposit was simulated with the 1D hydrodynamic code ESTHER, which leads to the knowledge of thermodynamic paths followed by the plasma plume during and after the laser pulse over a period of 3750 ns. This numeric tool is associated with a nucleation model calculating the size of the formed nanoparticles. It is now accepted that nanopowders formation in expanding plasmas is mainly due to the non-equilibrium condensation [5,9]. Indeed, during the plasma plume expansion both temperature and density decrease, thus the thermodynamic path crosses the liquid–gas saturation curve, i.e. the binodal. Typical expansion velocity is of a few tens of km h^{-1} [1,10], so that the hydrodynamic expansion time may be shorter than the equilibrium condensation time. Three configurations are possible according to the efficiency of the laser heating. For laser fluences below about 0.4 GW cm^{-2} in our experimental conditions, heating is not efficient enough to produce a high velocity expanding plasma and condensation cannot take place even in equilibrium conditions. A liquid–solid mixture is produced at the target surface and micrometric debris are ejected at small velocities. This situation can also be found for larger fluences at the periphery of the interaction region due to the spatial energy distribution in the laser spot. Condensation can only take place when the thermodynamic path crosses the non-equilibrium saturation curve (the binodal). It must be noticed, however, that the laser fluence is limited to that required for ambient air ionization, i.e. a few GW cm^{-2}. In this situation, a self-regulated regime exists where ablation velocity does not increase any more with laser irradiance, which is partially absorbed in the ambient air. This self-regulated situation is complex and should be avoided to ensure accurate diagnostics.

Condensation is a typical non-equilibrium supersaturation process, which occurs during the expansion of the plasma plume when it reaches the spinodal. This possibility to obtain non-equilibrium condensation is shown in Fig. 1a which displays the thermodynamic paths obtained for a 4.78 J cm^{-2} laser shot at a wavelength $\lambda = 1064$ nm on a titanium target. Several pulse durations were used for these calculations, τ_p(FWHM) = 40, 10, 5 and 1 ns, corresponding to a laser irradiances $I_p = 0.12$, 0.48, 0.96 and 4.8 GW cm^{-2}, respectively.

Heating and subsequent hydrodynamic processes take place simultaneously from the beginning of the laser pulse. At very short duration pulse, laser energy is mainly used to expand the solid and to vaporize it producing a liquid–gas mixture. In the case of 10 ns pulse duration (Fig. 1a (bottom)), the saturation curve is crossed and the plasma gas produced is heated up to about 7000 K for a time $t = 22$ ns. Then the gas, i.e. the plasma, expands in the ambient air where the binodal is crossed again. At this point, thermodynamic conditions are favorable to non-equilibrium vapor condensation, i.e. nuclei formation [11]. These phenomena have been widely studied in the case of fs-lasers, but in the nanosecond regime more complex hydrodynamic processes take place. Moreover, in this work the laser/target interaction is carried out in an ambient gas which has a counter-pressure effect. A shock wave is generated in the ambient air because of the expansion of the plume, which modifies the adiabatic expansion. Fig. 1a (bottom) shows the thermodynamic path in the region of the saturation domain. From $t = 9$ ns to 11 ns, the shock wave produced by laser energy deposition interacts with the plasma plume/air contact surface, which enhances heating and compression. Then, the shock wave crosses the contact surface, which relaxes pressure up to a time of 12 ns. Temperature follows increasing up to a time $t = 22$ ns. Then, the plasma plume expands quasi-adiabatically, the edge of expansion wave being shocked to a pressure which depends on the ambient gas pressure. Condensation can start at about 255 ns, which corresponds to a distance of a hundred of micrometers from the target

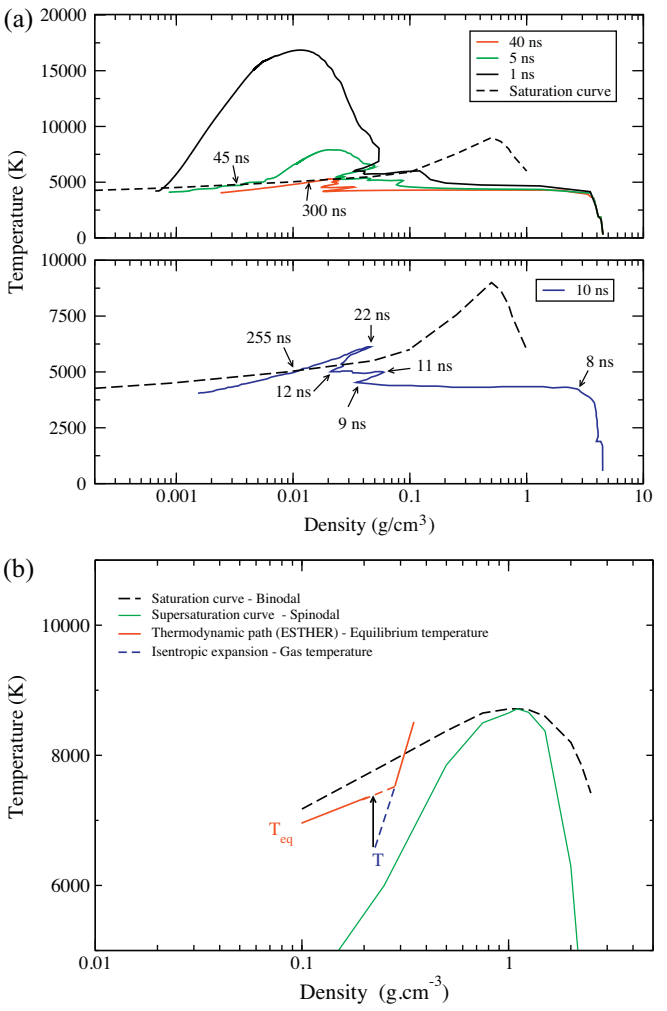

Fig. 1. (a) Calculated thermodynamic paths for the contact surface between plasma and ambient air for a laser pulse operating at 1064 nm with a fluence of 4.78 J cm^{-2}. Several pulse durations, τ_p, were used: (top) 40, 5 and 1 ns (bottom), 10 ns. Characteristic times of the plasma plume evolution are indicated. (b) Schematic representation of the saturation parameter θ_{max} for a gas temperature T and an equilibrium temperature T_{eq}.

surface. It can be seen that the saturation temperature decreases when the irradiance increases, which can modify subsequent nucleation conditions. Indeed, the gap between binodal and spinodal curves increases when temperature decreases. For a given expansion time of the plume, the residence time in the non-equilibrium region increases, which leads to the growth of larger nuclei.

Now, we address the possibility to obtain particles a few nanometers in size. A simple criterion proposed first by Zel'dovich and Raizer [11] enables to express the saturation degree θ. This parameter is directly linked to the notion of saturation pressure, which can be calculated by using the Clausius–Clapeyron law. According to the previously described thermodynamic paths, powders formation is mainly due to a non-equilibrium condensation mechanism of plasma [12]. Moreover, we assume that condensation process is homogeneous. So, condensation centers are formed and collisions between particles can induce agglomeration. In other words, a first liquid droplet, i.e. a nucleation center, is formed, then it grows by sticking of others liquid particles. Depending on the thermodynamic path followed by the plasma, the produced particles will display different sizes and structures. The higher the irradiance, the more the plasma relaxes and the higher the gap between binodal and spinodal curves at equilibrium is. However,

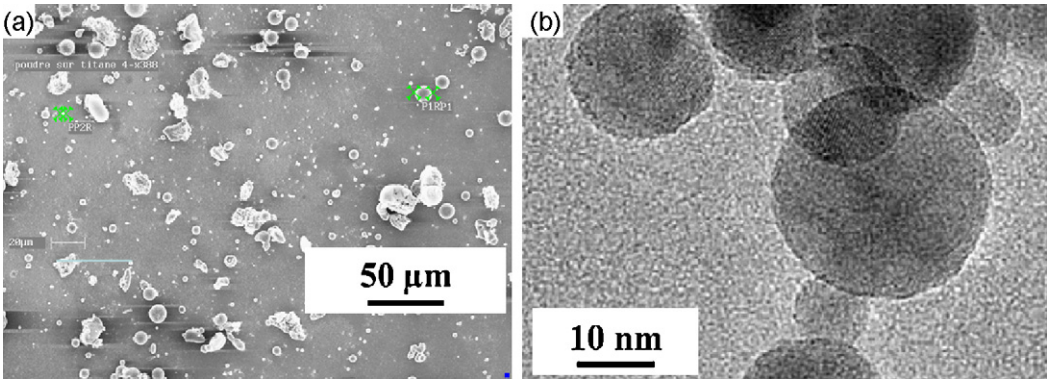

Fig. 2. Electron microscopy views of powders collected during the laser treatment of a titanium target: (a) SEM view showing micrometric particles, (b) TEM image showing nanoparticles.

as it was explained before, a maximum fluence value exists which corresponds to the direct ionization of the ambient air. This leads to a particular nuclei production away from equilibrium conditions.

At the supersaturation limit (spinodal), condensation reaches its maximum, characterized by the maximum saturation degree, θ_{max}. The maximum condensation rate is reached and the size of the formed nuclei corresponds to a critical radius, r^*, which is the smallest radius of a condensation center, so it is the radius of the first formed liquid droplet. Then, the equilibrium curve (binodal) is reached very quickly. For a given plasma density, ρ, the degree of saturation, θ, is defined by [11]:

$$\theta = \ln\left(\frac{T_{eq}}{T}\right) \simeq \left(\frac{T_{eq} - T}{T_{eq}}\right) \quad (1)$$

where T_{eq} is the equilibrium temperature calculated with the ESTHER code by using an equilibrium equation of state, and T is the expanding plasma temperature determined by extending the isentropic expansion curve in the non-equilibrium zone (Fig. 1b). For a given saturation degree, the nuclei formation rate, $I(\theta)$, corresponds to the number of condensation centers per vapor atom and per time unit, assuming a constant supersaturation [11]. The maximum value of $I(\theta)$ corresponds to the highest nuclei formation rate and the highest saturation degree, θ_{max}. The critical radius r^* is related to θ_{max} by the equation [11]:

$$r^* = \frac{2\sigma\omega R}{kL_{vap}\theta_{max}} \quad (2)$$

where σ is the surface tension, ω is the volume of liquid per molecule, R is the gas constant, L_{vap} is the vaporization heat and k is the Boltzmann constant. It must be emphasized that r^* is not an average value but the radius at the condensation maximum. Once the maximum saturation degree θ_{max} is reached, condensation continues thanks to new liquid droplets. Centers growth can continue by condensation or by sticking. In order to simplify the equations, we consider separately each process. The droplet growth rate by condensation, g_{cond}, can be calculated from the kinetic theory of gases with the Hertz–Knudsen model [9]. Contrary to condensation, the growth rate by sticking, g_{stick}, can be modeled with a continuous approach which takes into account scattering before cohesion of individual particles. Growth rates are calculated at the maximum saturation degree, θ_{max}.

3. Results and discussion

3.1. Experimental characterization of the collected powders

Fig. 2 shows typical electron microscopy images of powders collected on a glass plate during the laser treatment on a Ti target with the experimental conditions described in Fig. 1, namely laser fluence equal to 4.78 J cm^{-2}, τ_p (FWHM) = 40 ns and irradiance I_p = 0.12 GW cm^{-2}. SEM observations (Fig. 2a) show that powders are composed of micrometric particles together with quite smaller particles forming an almost continuous layer. TEM observations (Fig. 2b) show nanoparticles less than 30 nm in diameter. Nanoparticles are mainly composed of titanium dioxide, TiO_2, in anatase or rutile phases depending on the nanoparticle size. It is worth to note that the structure of TiO_2 nanoparticles changes from the anatase to the rutile phase for particle sizes above 15–20 nm.[8,13]

Micrometric particles are only collected near to the target surface due to their larger mass which limits the free-fly time. These micrometric particles are ejected from the plasma mixture after crossing the saturation domain.

3.2. Modeling the influence of the ambient gas

Aside from the thermodynamic paths, the ESTHER code enables to analyze the formation of nanoparticles as a function of different experimental parameters related to the laser irradiation conditions and the nature of the sample. Moreover, the chemical nature and the pressure of the ambient gas are also important parameters to be studied.

In order to study of the influence of the ambient gas molar weight, we have done ESTHER simulations with the same laser irradiation conditions reported by Clair et al. [14,15] in a experimental study using argon as ambient gas. Copper (Cu) was used as a target and the laser parameters were the following ones: fluence 18.8 J/cm^2, τ_p(FWHM) = 6 ns, irradiance I_p = 3.1 GW/cm^2.

The positions of both the shock wave and the contact surface were calculated with the ESTHER code and compared to the experimental results obtained by spectroscopy diagnostics and thermal emission, respectively. Fig. 3 shows a good agreement between calculated and experimental results. Then, ESTHER simulations have been done using air as ambient gas. Results are compared in Fig. 3b with those obtained using argon as ambient gas. They show the influence of the ambient gas molar weight. Shock waves, as well as plume velocities, decrease with the inverse of molar weigh ratio, as expected by Hugoniot's relations. This shows that the number and the diameter of nuclei can be modified by the increase of ambient gas molar weight, which modifies the expansion path.

3.3. Modeling nanoparticles formation

Fig. 4 shows the calculated saturation degree, θ, as a function of the plasma density with the laser irradiance values used in Fig. 1 in the case of 5 and 10 ns pulse durations. In these conditions, the saturation curve is crossed and adiabatic expansion can get into in the

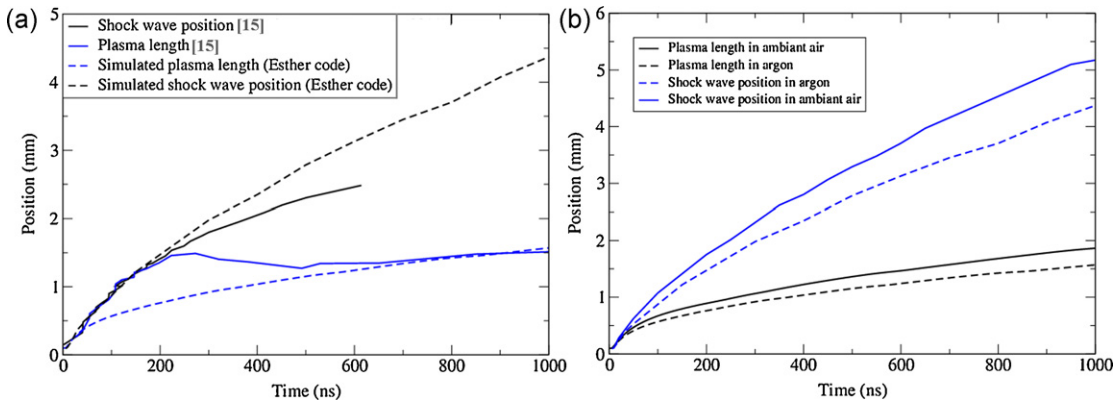

Fig. 3. Plasma plume edge and shock-wave positions: (a) ESTHER simulations and experimental measurements [14] for laser treatments using argon as ambient gas, (b) comparison of ESTHER simulations using argon and air as ambient gas.

non-equilibrium saturation zone, as confirmed by the evaluation of the saturation parameter θ (Eq. (1)). For 10 ns pulses, it is shown that condensation begins earlier, at a higher density than in the case of 5 ns pulses. Moreover, the maximum saturation parameter is higher, which means that particles have more time to nucleate and condensate. This is confirmed by plasma plume velocity which is two times smaller with 10 ns pulses [1].

For a pulse duration of 40 ns, laser irradiance, i.e. heating conditions, is not enough to reach condensation conditions (Fig. 1). Indeed, the thermodynamic path stays very close to the saturation curve. Thus, it is a critical regime, where condensation is low. On the other hand, in the case of 1 ns pulses, the thermodynamic path crosses the saturation curve, but the adiabatic expansion is not long enough to apply the previous model.

For pulse durations of 5 and 10 ns, we have calculated the condensation parameter, θ_{max}, the critical radius, r^*, the condensation and sticking rates, (g_{cond} and g_{stick}, respectively), the total number of condensation centers formed either by condensation or by sticking, which gives an estimate of the final particle radius $r_{nucleus}$. Furthermore, the model allows to estimate the onset time, Δt, corresponding to the saturation parameter, and the height above the surface where particles are formed, h_{powder}. All these results are summarized in Table 1.

Firstly, the calculated values of g_{cond} and g_{stick} show that condensation is the dominant mechanism leading to the increase of nuclei radius. Indeed, for both pulse durations g_{stick} is about 1, whereas g_{cond} is about a few hundreds. The final particle radius was estimated about 1 and 5 nm, for laser pulses of 5 and 10 ns, respectively.

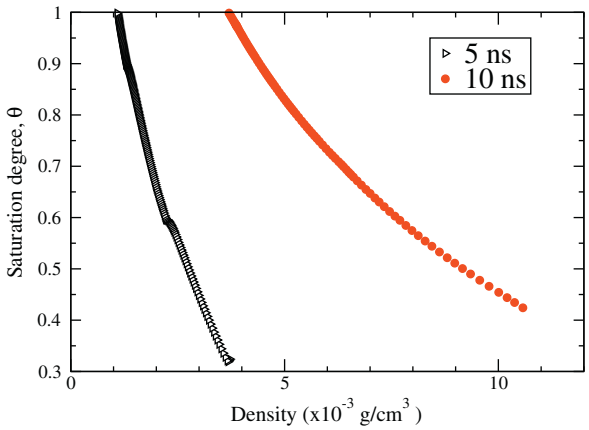

Fig. 4. Saturation degree, θ, as a function of the plasma density for pulse durations of 5 and 10 ns.

Table 1
Simulation results obtained for 5 and 10 ns laser pulses with the ESTHER code coupled with a nucleation model: the total number of condensation centers created by condensation, g_{cond}, the condensation centers radius, r^*, the final nucleus radii, $r_{nucleus}$, the onset saturation time, Δt, and the height above the target surface where particles are formed, h_{powder}.

τ_p (ns)	Irradiance (GW cm^{-2})	g_{cond}	r^* (nm)	$r_{nucleus}$ (nm)	Δt (ns)	h_{powder} (mm)
10	0.48	154	0.09	4.7	1780	3.0–4.0
5	0.96	308	0.18	1.2	600	0.7–1.5

Thus, decreasing the laser irradiance, increases the radius of the nuclei population. We can also notice that the radius of condensation centers for 5 ns pulses is larger than that for 10 ns pulses. On the other hand, the residence time Δt in the non-equilibrium zone is longer in the case of 10 ns pulses, which leads finally to bigger nuclei for 10 ns pulses. Furthermore, these results show that condensation mechanism is faster for short pulse durations. Numerical simulations allow also to estimate the height above the target where the particles are formed (Table 1) taking into account the shock wave position and the plasma height at the maximum saturation degree θ_{max}. We can conclude that the higher the irradiance, the closer to the target the particles are formed. Finally, similar trends are expected by increasing the pressure or the molar weight of ambient gas which will reduce the plume expansion velocity in a similar way that the irradiance decrease.

4. Conclusions

The hydrodynamic code ESTHER, coupled with a nucleation model, has been applied for determining the conditions leading to the nanoparticles formation in the plasma plume induced by nanosecond pulsed laser treatment of metal targets. The sizes of condensation centers and resulting nuclei, the condensation rate and the height above the target where nanoparticles are formed have been calculated by this method. Two main conclusions can be drawn: firstly, the nuclei size increases when the laser irradiance decreases, and, secondly, the higher the irradiance, the closer to the target the particles are formed.

Acknowledgments

The authors would like to thank Conseil Régional de Bourgogne, France, for its financial help in this research program. The authors acknowledge the financial support of this work provided by 'Grand Chalon', France.

References

[1] M. Cirisan, J.M. Jouvard, L. Lavisse, L. Hallo, R. Oltra, Journal of Applied Physics 109 (2011) 103301.
[2] S. Amoruso, G. Ausanio, R. Bruzzese, M. Vitiello, X. Wang, Physical Review B 71 (2005) 033406.
[3] M. Vaezzadeh, M. Saeidi, M. Zarei, Physica E 42 (2010) 1787–1789.
[4] S.C. Singh, R. Gopal, The Journal of Physical Chemistry C 112 (2008) 2812–2819.
[5] E. Lescoute, L. Hallo, D. Hébert, B. Chimier, B. Etchessahar, V.T. Tikhonchuk, J.-M. Chevalier, P. Combis, Physics of Plasmas 15 (2008) 063507.
[6] M.F. Becker, J.R. Brock, H. Cai, D.E. Henneke, J.W. Keto, J. Lee, W.T. Nichols, H.D. Glicksman, Nanostructured Materials 10 (1998) 853–863.
[7] J.P. Colombier, P. Combis, F. Bonneau, R. Le Harzic, E. Audouard, Physical Review B 71 (2005) 165406.
[8] I. Shupyk, L. Lavisse, J.M. Jouvard, M.C. Marco de Lucas, S. Bourgeois, F. Herbst, J. Piquemal, F. Bozon-Verduraz, M. Pilloz, Applied Surface Science 255 (2009) 5574.
[9] E. Lescoute, L. Hallo, B. Chimier, D. Hébert, V.T. Tikhonchuk, C. Stenz, J.-M. Chevalier, J.-L. Rullier, S. Palmier, The European Physical Journal Special Topics 175 (2009) 159–164.
[10] D.B. Geohegan, A.A. Puretzky, G. Duscher, S.J. Pennycook, Applied Physics Letters 72 (1998) 2987.
[11] Y.B. Zel'dovitch, Y.P. Raizer, Physics of Shock Waves and High-Temperature Hydrodynamic Phenomena, Dover Publications, 1960, pp. 585–595.
[12] M.S. Tillack, D. Blair, S.S. Harilal, The effect of ionization on cluster formation in laser ablation plumes, UCSD report UCSD-ENG-103, 2003.
[13] Y. Hu, H.-L. Tsai, C.-L. Huang, Materials Science and Engineering A 344 (2003) 209.
[14] G. Clair, PhD Thesis, Université Aix-Marseille, France, 2011.
[15] G. Clair, D. L'Hermite, Journal of Applied Physics 110 (2011) 083307.